DEVELOPMENT OF OIL DOT VISUALIZATION TO MEASURE THE SHEAR STRESS

G. Bonfanti
Aerospace Department
Politecnico di Milano
Milano, Italy

T. Yasa, S. Lavagnoli, G. Paniagua
von karman Institute for Fluid Dynamics
Rhode-St-GenèseBelgium
e-mail : paniagua@vki.ac.be

ABSTRACT

This paper presents an innovative technique for shear stress measurement based on conventional oil dot visualization. The deformation of the oil dots during the experiments is recorded by means of a CCD camera. Tests were carried out for several flow velocities in a free jet. A computer code was developed to calculate shear stress based on deformation speed. The results were also compared with theoretical calculations. The new technique is quite promising for the measurements of flow speed and wall shear stress.

INTRODUCTION

The evaluation of the wall shear stress is of utmost importance to determine the boundary layer status and drag. For a newtonian fluid the stress is proportional to the dynamic viscosity of the flow and to the velocity gradient as given in Eq. 1

$$\tau_w = \tau\big|_{y=0} = \mu \cdot \frac{\partial u}{\partial y}\bigg|_{y=0} \qquad (1)$$

Some precise techniques are capable to measure the wall shear stress comprise diverging fringe shear stress sensor (OFI) [1] and the micro-pillar shear-stress sensor (MEMS) [1]. The first technique relies on the principle that the rate at which oil thins on a surface is a function of the shear stress magnitude. The interference between the partially reflected light, coming from a light source, at the air-oil interface and the light reflected from the model surface will vary as the oil film thickness changes. This is observed as a series of light and dark bands or fringes, the spacing of which is proportional to the skin friction. The second refers to micro-electromechanical system. It uses sensors to measure the integrated force produced by wall shear stress on a flush mounted movable floating element. The floating element is attached to either a displacement transducer or is part of a feedback force rebalance configuration. The output signal is proportional to the acting shear stress according to the physical low. However, the implementation of these methods is rather complex and prevent their routinely application to the turbomachinery field.

Some rude techniques for flow visualizations were introduced by Leonardo da Vinci in the XVI century. Later, scientists like Mach, Reynolds, Prandtl, von Kármán, and Taylor contribute to the development of the technique. The simplicity and the low cost allow its implementation in a vast variety of applications. Tian et al. [2] carried out surface oil flow visualizations on the endwall flow of a low speed linear cascade wind tunnel. It was the first time that quantitative measurements of the oil-flow direction and wall shear stress were measured and compared using laser doppler anemometry. Atsushi et al. [3] measured the shear stress distributions over a fan blade using the oil-film visualization technique combined with image analysis. The surface velocity of the oil-film over the blade surface is measured by cross-correlating two images with a certain pattern displacement. The transformation of the surface velocity to shear stress is made by a well known shear stress distribution over a rotating disk, which allows the correction of centrifugal force effect on the surface velocity of the oil film. Naughton [4] developed high quality skin friction measurements in two-dimensional flows using oil film interferometry, on a hump mounted on a splitter plate. The results obtained indicate that, at least in two-dimensional flows, Oil Flow Interferometry may be effectively used for a wide range of settings. Ito and Oyangi [5] computed an approximate estimation of the skin friction using the oil dot method. They propose an approximate skin friction estimation method that uses tracking oil dot movement. The method uses the correlation between oil dot velocity and skin friction obtained by measurement on flat plate laminar boundary layer in a wind tunnel. The results obtained show that approximate skin friction values on aerodynamic bodies can be easily estimated by this method.

The present work aims to use the oil visualization method not only for qualitative streamline tracing but also to get some quantitative data. Since the movement of the oil depends on the flow velocity and some other parameters (i.e. viscosity of the oil, surface tension, pressure

gradient, gravity, etc…) it is possible to get quantitative information by monitoring the oil displacement during a test. The testing is carried out with a flat plate on a vertical free jet facility. Images of dot's movements are analyzed and the shear stress results obtained compared with theoretical value. The investigation carried out is a solid base to improve this promising technique.

NOMENCLATURE

g	Gravity acceleration [m/s^2]
H	Observation window
h	Dot's height [m]
i	Current frame
P	Pressure [Pa]
Re$_x$	Local Reynolds number ($\rho\, U_\infty\, x\, /\, \mu$)
t	Time [s]
T	Temperature [K]
u	Boundary layer flow speed [m/s]
U	Velocity x-direction [m/s]
W	Velocity z-direction [m/s]
x	Longitudinal direction [m]
y	Perpendicular direction to the plane
z	Perpendicular direction to x and y

Greek

τ_w	Wall shear stress [N/m^2]
μ	Dynamic viscosity [Pa·s]
ρ	Density [Kg/m^3]
υ	Kinematic Viscosity [m^2/s]

Subscripts

c	Convective term
∞	Free-stream quantity

MEASUREMENT TECHNIQUE

Theoretical Background

Flow visualization is the art of making flow patterns visible. Colored oil sheets, lines or dots can be used to identify the surface streamlines of the flow. Considering an oil dot, it is possible to approximate its deformation as illustrated in Figure 1.

Figure 1: Oil film in air flow, showing initial and final positions

An oil film on a solid surface generally moves under the action of gravity, pressure gradient, surface tension and skin friction resulting from the airflow over the oil surface. It is demonstrated [1] that if the film is thin enough (less than 10μm) the dominant effect is the skin friction and the other terms can be neglected.
The thin oil film theory and the relative equations were originally derived by Squire [6] when he considered the motion of oil acted upon by shear.

Squire's results showed that, except in the case of separated flows, the moving oil follows the streamlines and influences very little the boundary layer properties. Squire provided the basis for the shear stress measurement technique based on oil films, but Tanner and Blows [7] pioneered the first practical application of the thin oil film equations.
In order to derive the equations that govern the motion of a thin oil film, a control volume is defined considering a small element of convected oil film as shown in Figure 2.
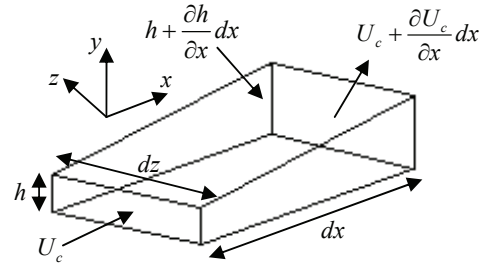

Figure 2: Control volume for developing the thin oil film equations [9]

Considering two-dimension mass balance of the oil film and momentum equation in flow direction, the Eq 2 can be obtained by neglecting inertial and viscous terms.

$$0 = -\frac{\partial P}{\partial x} + \frac{\partial}{\partial y}\left(\mu\frac{\partial u}{\partial y}\right) + \rho g_x \qquad (2)$$

It should be noted that the term between parentheses is the shear stress ($\tau_{w,x}$) in case of a Newtonian fluid.
If Eq. 2 is integrated in y-direction and the boundary conditions are applied, the velocity in the x-direction is expressed as in Eq. 3. The boundary conditions are defined as follows; the oil velocities are equal to those in the boundary layer at the surface of the oil and the viscous stresses has equal values in both side of the oil/air interface. Additionally, the oil body is assumed to be stationary.

$$u = \frac{1}{\mu}\left(\frac{\partial P}{\partial x} - \rho g_x\right)\left(\frac{y^2}{2} - hy\right) + \frac{\tau_{w,x}}{\mu} y \quad (3)$$

In order to determine the convective velocity (U_c) Eq. 3 is integrated in y-direction between the wall and the oil film surface, thus obtaining:

$$U_c = \frac{1}{h}\int_0^h u\, \mathrm{dy} = \frac{\tau_{w,x}h}{2\mu} - \frac{h^2}{3\mu}\left(\frac{\partial P}{\partial x} - \rho g_x\right)(4)$$

Repeating the analysis for the z-direction it yields:

$$W_c = \frac{1}{h}\int_0^h w\, \mathrm{dy} = \frac{\tau_{w,z}h}{2\mu} - \frac{h^2}{3\mu}\left(\frac{\partial P}{\partial z} - \rho g_z\right)(5)$$

Combining the mass balance of the film and Eq. 4-5 the thin film equation is obtained by Squire as shown in Eq. 6 by neglecting the pressure gradients and the gravitation.

$$\frac{\partial h}{\partial t} + \frac{\partial}{\partial x}\left(\frac{\tau_{w,x}h^2}{2\mu}\right) + \frac{\partial}{\partial z}\left(\frac{\tau_{w,z}h^2}{2\mu}\right) = 0 \quad (6)$$

Eq. 6 shows that the dominant force that acts on a thin film is the skin friction. This equation also takes into account the film thickness variation and the skin friction distribution.

Tanner and Blows [7] have developed an alternative form of the Eq. 6:

$$\tau(x) = \frac{2\mu}{ty^2}\int_0^x y\ dx \quad (7)$$

Equation 7, equivalent to the Squire's form (Brown and Naughton [8]), has the advantage to readily compute the wall shear stress once the viscosity, displacement and thickness of the oil dot are known.

For these reasons it is strictly necessary to have precise measurements of the oil's mixture viscosity. Recording the dot displacement during the test by means of camera it is possible to reconstruct its thickness evolution. As all the terms of Eq. 7 are noted, it is possible to compute the wall shear stress.

Data Processing

A post-processing tool has been developed using the Matlab image processing toolbox in order to analyze the oil film deformation on acquired images. The code loads the full video and performs frame by frame analysis. A chosen dot is analyzed each run. A flow diagram of the algorithm is reported in Figure 3.
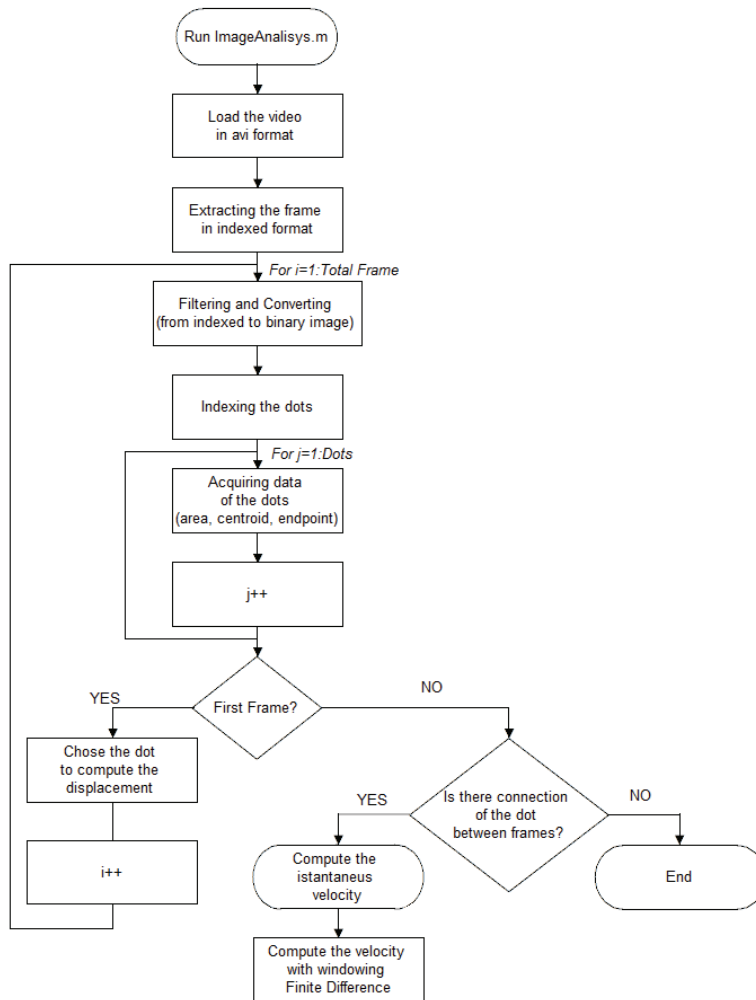

Figure 3: Block scheme of the implemented algorithm

The program converts the indexed frame to a binary image. Filtering is applied in order to increase the quality of the conversion. First of all, the spots that have a radius below a certain threshold are removed from the image. Then, the remaining spots are identified as oil dots and are indexed so that the same dot can be tracked down in the following frames.

The dot to be analyzed is chosen from the dots recognized in the first frame. Then, the same dot is traced over the movie in order to compute its surface area, center and endpoints for each frame. The endpoint represents the coordinate of the last pixel of the select dot along the longitudinal axis of the plate. The deformation velocity is calculated considering the endpoint evolution of the oil dot. Two methodologies are examined for the velocity calculation. Initially, a finite difference first order forward scheme is used for the calculation. However, the image resolution is an important issue for this technique. If the image resolution is poor at high shutter speed, the oil border remains in the same pixel although it moves. It causes artificial velocity variation in the final results (Figure 4 (up)). Therefore the preceding scheme is replaced with a forth order finite difference scheme. It uses information coming from five frames (Eq. 8) as shown in Figure 5. A better approximation is obtained if there is a movement in the dot's edge of one pixel between two acquired frames. The sampling rate is also reduced by half by re-sampling the data. The implementation of a finite difference algorithm shows a smoothed trend in the velocity evolution (Figure 4 (down)).
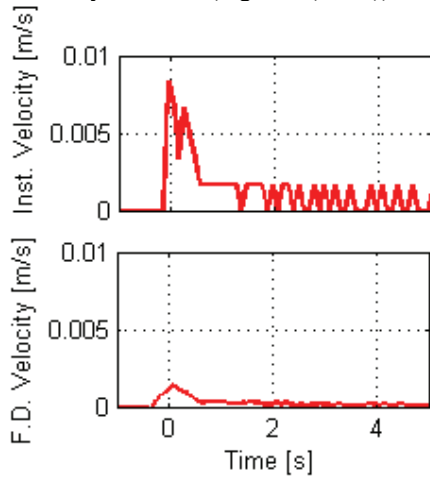

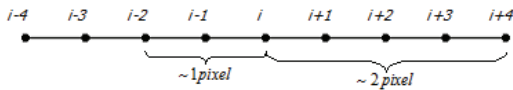**Figure 4: Instantaneous velocity and finite difference approximation**

Figure 5: Finite difference scheme adopted

$$u(i) = 4.17 \cdot 10^{-4} \cdot x(i - 4 \cdot h) - 3.33 \cdot 10^{-3} \cdot x(i - 2 \cdot h) + \qquad (8)$$
$$+ 3.33 \cdot 10^{-3} \cdot x(i + 2 \cdot h) - 4.17 \cdot 10^{-4} \cdot x(i + 4 \cdot h)$$

Once the velocities are obtained as pixel/frame, they are converted first to pixel/s using the sampling rate, then m/s using a reference image. The reference image is obtained recording a frame of the target object covered by a thin millimetric

paper sheet once the optical setup is set. The reference image allows then one to accurately estimate the size of each pixel.

The computation of the wall shear stress along the longitudinal axis of the plate is based on the assumptions of the thin sheet theory and Eq. 7. Since it is not possible to use interferometry during the test, the oil dot thickness is estimated assuming that the oil film shape evolves as illustrated in Figure 6. Therefore the initial shape of the dot is considered to be semi-spherical.
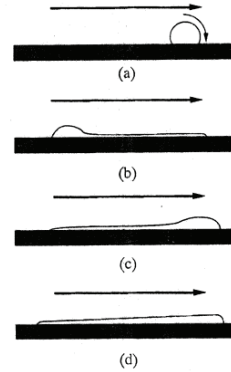

Figure 6: Patterns of oil dot movement

It is possible to compute the radius and the volume of the oil since the area is known from the images. This volume is unaltered during the deformation process because of constant oil density. Assuming the final layout of the dot with a certain slope of the thickness proportional to its longitudinal deformation (Figure 7), it is possible to calculate the final thickness of the oil sheet. Finally, the wall shear stress is obtained since all parameters in Eq. 7 are available.
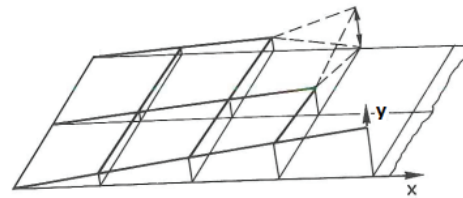

Figure 7: Approximation of the oil sheet evolution

Characterization of the oil mixture

The viscosity plays a fundamental role in the wall shear stress calculation. It is therefore important to have a precise characterization of the viscosity of the oil used. Dynamic viscosity is measured with various types of viscometer or rheometer. In the current case the viscosity has been measured with the Wells-Brookfield Digital Viscometer DV-II. The operating principle is based on the rotation of a sensing element in a fluid to measure the torque necessary to overcome the viscous resistance to the induced movement. This is accomplished by driving the immersed element, which is called spindle, through a beryllium copper spring. The

degree to which the spring is wound, detected by a rotational transducer, is proportional to the viscosity of the fluid.

The constraint for the current application is that the final oil mixture has to stand on a vertical surface without creeping under the gravitational force but it has to move during the test. This implies that the mixture should have a low limit for viscosity ($\mu>105$ Pa·s). It is possible to modify the viscosity of the oil by mixing it with a certain amount of pigments.

The oil is prepared by mixing the oil base with pigments using a magnetic mixer (Figure 8 (e)). The quantity of colored pigment is weighted by means of a precise digital balance. The pigment is selected as the micrometric's titan-bioxide (TiO_2) which presents a sharp contrast during the experiments (Figure 8 (f)).

Figure 8: The viscosity measuring system: spindle/chamber/heat exchanger (a-b), water bath of the heat exchanger (c), viscometer layout (d), magnetic mixer (e), TiO_2 (f)

Since the viscosity of a fluid is strictly dependent on the temperature, a detailed characterization is carried out. The measurements chamber is surrounded by an heat exchanger (Figure 8 (a) and (b)) that is connected to a heated water bath (Figure 8 (c)).

The Newtonian behavior of the base oil and the oil mixture is also tested by changing the rotational speed of the spindle at a fixed temperature. The results are compared with the literature in order to identifying the nature of the liquid.

Two different base oils are examined. First of all, a mineral oil with low viscosity is used as a first base liquid. The characterization of the mineral oil is performed (Figure 9 (up)). Then, 3 g of TiO_2 is added to the oil to have final paint. The results for the final mixture are depicted in Figure 9 (down).

However when the pigment is mixed with it, the mixture separates after a certain time. Therefore, accurate measurements are not performed for the mineral oil mixtures that contains higher rate of pigments. Furthermore, such substance is not suitable for the flow visualization as the pigments do not correctly follow the flow. Hence, the oil base has been changed with high viscosity silicon oil.
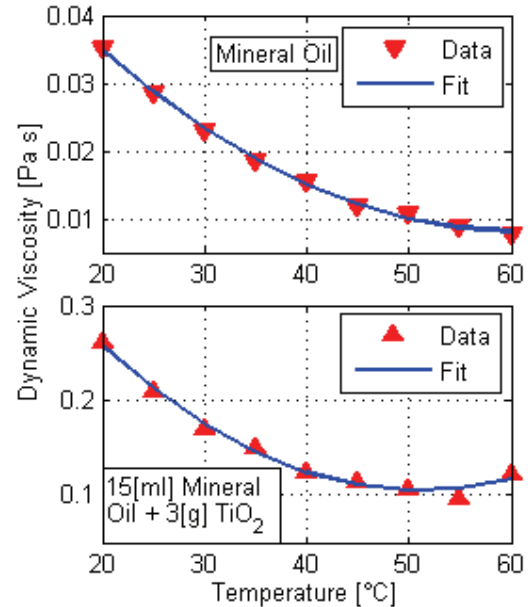

Figure 9: Viscosity characterization with temperature of mineral oil (up) and final mixture (down)

The second mixture is prepared using a high viscosity silicon oil. The characterization curve of the base oil is presented in Figure 10 (up). The oil presents a viscosity level close to 0.97 Pa·s at 25 °C. However, the viscosity varies rapidly at low temperature levels. An increase of 20 °C (from 30 °C to 50 °C), the viscosity decreases approximately 25%. Figure 11 (up) shows the newtonian characteristic of the oil at 25 °C. The oil shows a newtonian behavior since the viscosity remain constant changing the velocity gradient. The second paint is obtained by adding 8 g of TiO_2 to the silicon oil. The viscosity level of such mixture satisfies the necessary criteria for experiments. It is also quite homogenous. It doesn't present any lumps. The characterization with temperature of the paint is reported in Figure 10 (down). The results show that for the same amount of temperature change viscosity decreases about 10%, assuring a better stability level respect to the base oil alone.
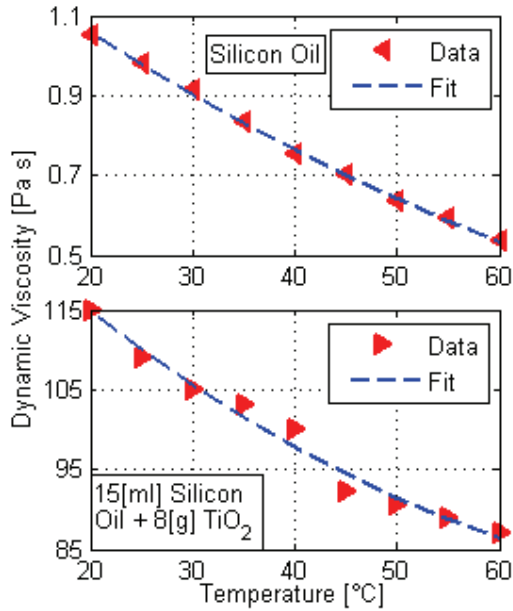
Figure 10: Viscosity characterization with temperature of silicon oil (up) and final mixture (down)

However adding the pigments changes the newtonian behavior of the silicon oil as depicted in Figure 11 (down). Fluids that show a decreasing viscosity with an increasing velocity gradient are classified as pseudoplastics.
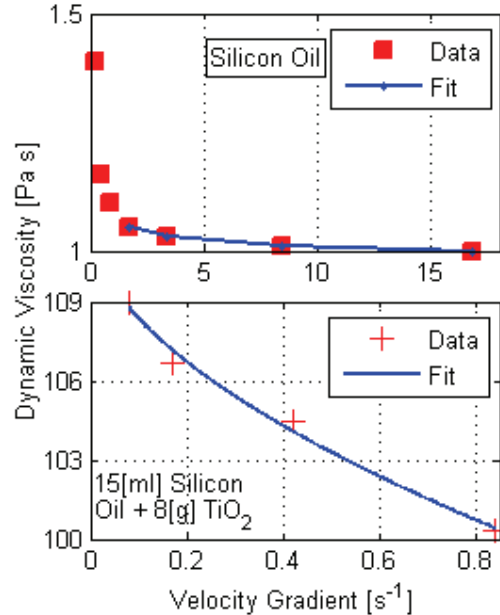

Figure 11: Variation of dynamic viscosity with velocity gradient of the silicon oil (up) and final mixture (down)

EXPERIMENTAL SETUP

The flow over a flat plate is a good test case to validate the oil dot technique since it is well characterized experimentally and theoretically in the literature. Therefore, a flat plate test bench is set up at the VKI free jet facility (Figure 12 (left)) to verify the applicability of the proposed methodology. The plate is vertically located in the jet. The velocity distribution on the plate is measured by means of pneumatic taps located to the center line of the plate. A shutter plate is placed at the exit of the jet. It allows setting the correct jet velocity before the oil deforms. The plate is monitored by means of a CCD camera. The images are recorded with a rate of 200 fps using the resolution of 800×600 pix. A light source heading to the flat plate is used in order to increase the contrast between dots and background. Figure 12 (right) shows the final test setup. The oil dots are manually placed next to the pneumatic tap locations. The manual deposition process makes difficult the estimation of the oil mass quantity. Hence, the final spot area is used to classify the dot dimensions. Figure 13 shows the final dot area for all experiments. Tests are performed at different velocities ranging from Mach 0.18 to 0.55. The tests are repeated several times to ensure the measurement repeatability.
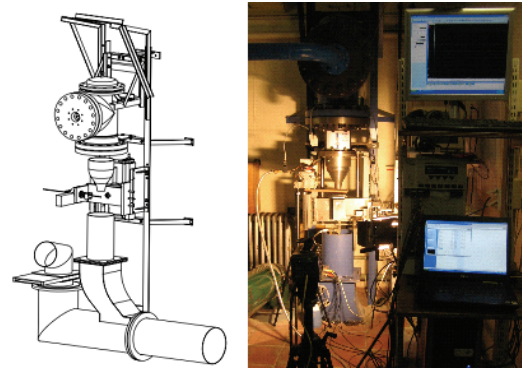

Figure 12: Sketch of the VKI free jet facility C4 used for the validation tests (left), Free jet facility equipped for the tests (right)
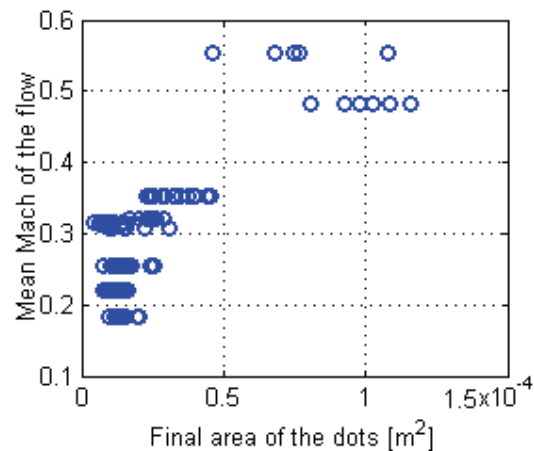

Figure 13: Final area of the dots

RESULTS AND DISCUSSIONS

Figure 14 displays the oil dot layout prior to a typical test. Each dot is identified and indexed with a number to keep track of its movement in the frame succession.
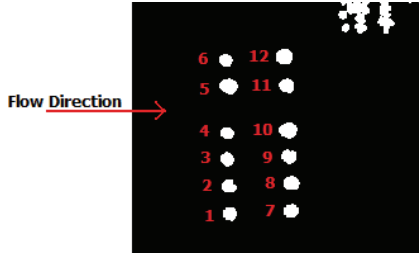

Figure 14: Dots reference order

The time evolution of Mach number on flat plate is plotted in Figure 15 (up) for four locations located along the plate central line. The velocity calculations are performed using compressible flow equation considering the atmospheric pressure and the settling chamber pressure. Before the opening of the shutter plate, the settling chamber pressure give slightly higher reading due to blockage of the shutter. When the shutter is actuated, the settling chamber pressure drops and stabilized after 1 s.
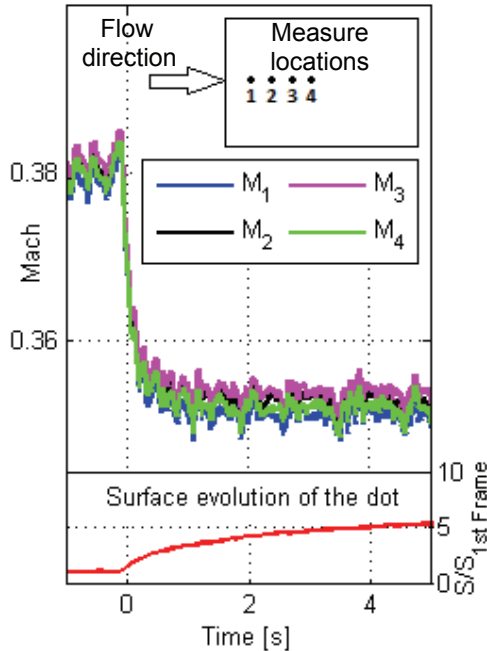

Figure 15: Time evolution of Mach number of the flow (up) and surface of the dot (down)

The deformation of a single oil dot is shown in Figure 15 (down). The area is normalized by the initial area of the dot. The rate of deformation is higher after the shutter opening due to the big quantity of oil on the spot. Once the oil spreads out, the rate of deformation decreases.

Figure 16 (up) and (down) shows in red the mean value of the velocity approximations of all the dots on the plate for two different jet velocities. All the dots have the same rate of velocity change independently on the plate location. This means that the small variation on the oil quantity does not have any significant effect on the deformation rate. The comparison between the velocity evolutions of the dots confirms that the phenomenon is repeatable. The computed deformation rate is also affected by camera resolution. High resolution images are needed at low deformation rate in order to increase the quality of the results. Therefore, the results at high velocity case (high deformation rate) shows cleaner trend than the one at low speed.
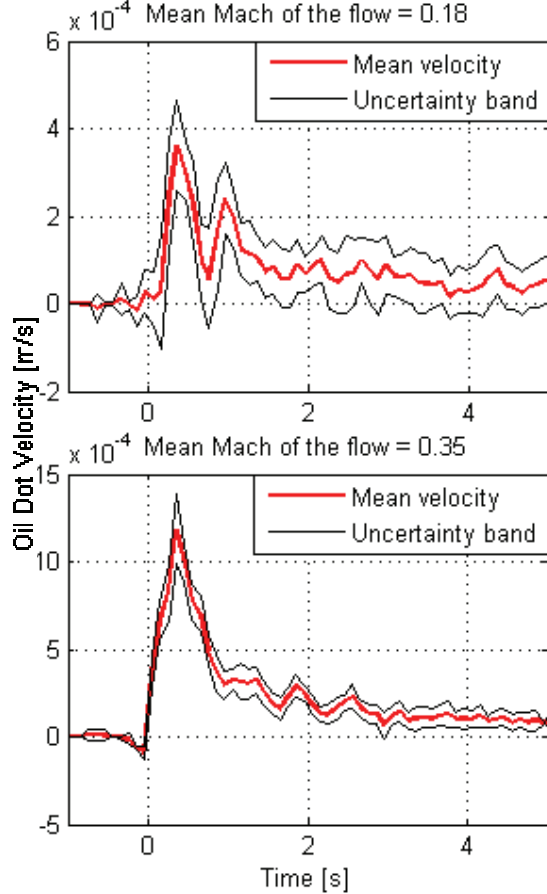

Figure 16: Oil dots velocity evolution in time: low flow speed test (up), high flow speed test (down).

The shear stress is computed using the Eq. 7 as previously illustrated. The results are reported in Figure 17 (a) and (b) in function of location and time, respectively. The thin sheet theory is not applicable for an oil dot at the initial time steps because the thin sheet theory is not satisfied. The thickness at the beginning of the test is around 2 mm and the technique is applicable when it is around 10μm. Hence, the high level of shear stress at the beginning is not considered. Once the dot forms a thin sheet, the technique starts giving meaningful values.

The boundary layer development on a flat plate is well documented for air flows. The theoretical wall shear stress is calculated using Blasius [9] equation (Eq. 9) for laminar flows whereas a correlation given by Eq. 10 [9] is used for the turbulent case.

$$\tau_w(x) = 0.332 \mu U_\infty \sqrt{\frac{U_\infty}{\upsilon x}} \qquad (9)$$

$$\tau_w(x) = \rho U_\infty^2 0.0296 \left(\mathrm{Re}_x \right)^{-1/5} \qquad (10)$$

The local Reynolds number for the dots are below $7 \cdot 10^5$ which remains in the laminar flow range ($5 \cdot 10^5 < \mathrm{Re}_x < 10^6$ [9]). However, this is just a theoretical estimation. In reality, it strictly depends on surface roughness, ambient condition, free-stream turbulence level, etc… Since all these parameters are not determined during the test, both the laminar and turbulent cases are considered.
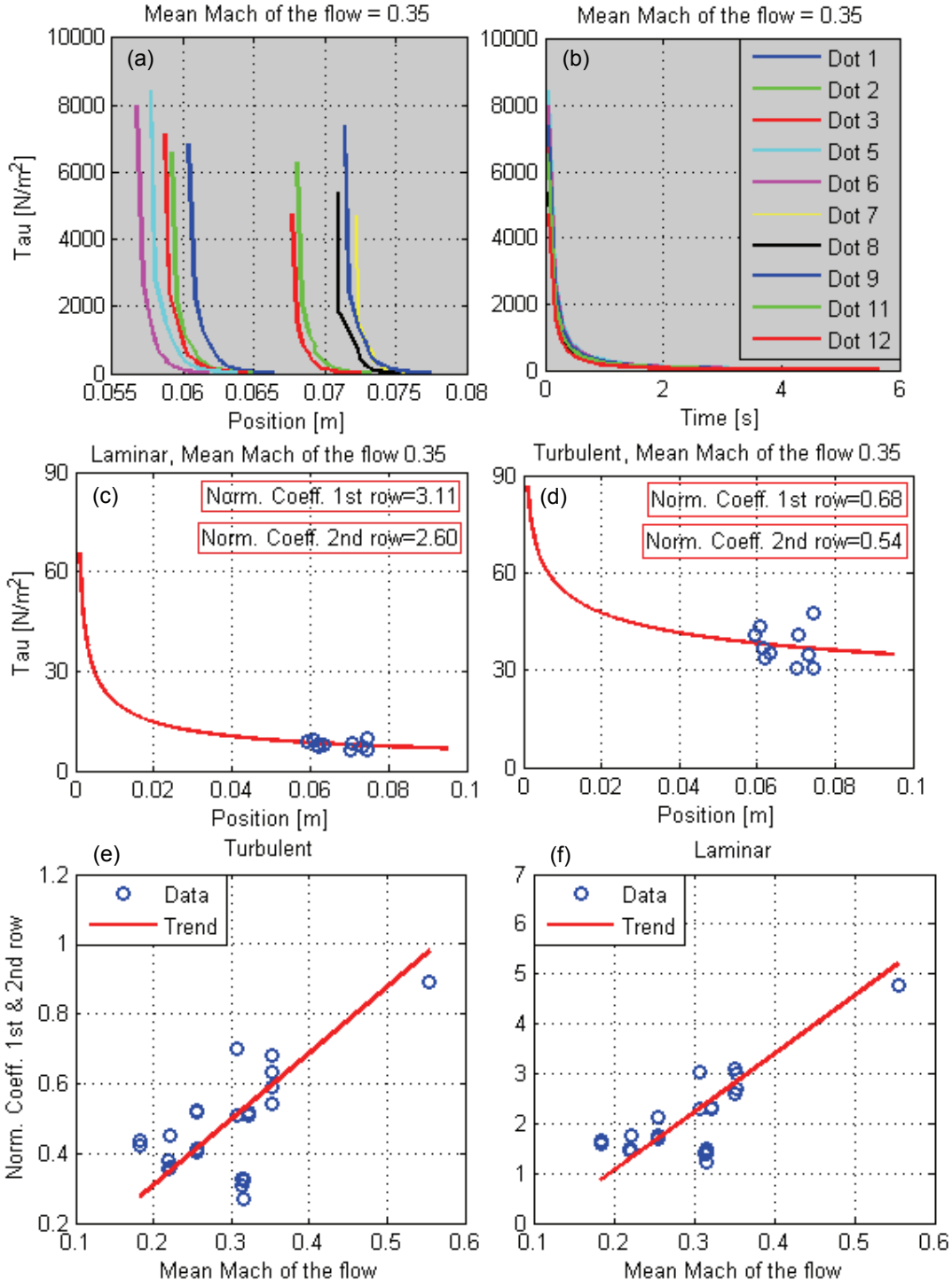
Figure 17: Shear stress evolution with position along the flat plate (a), Shear stress evolution with time (b), Experimental data and laminar shear stress evolution with position along the flat plate (c), Experimental data and turbulent shear stress evolution with position along the flat plate (d), Final trend of the normalization coefficient for the laminar case (e), Final trend of the normalization coefficient for the turbulent case (f)

Figure 17 (c) and (d) shows the theoretical and experimental comparison of the wall shear stress values for the laminar and turbulent case. The experimental data are obtained by averaging the shear stress values where the thin sheet theory is applicable. The experimental data are scaled down with a coefficient in order to have a comparison with the theoretical data.

The experimental results over-predict the theoretical values when laminar flow considered. On the other hand, they are lower than the turbulent flow estimations. The same comparison is done for all experimental data. Then, the evaluation of the normalization coefficient is plotted in function of flow velocity in Figure 17 (e) and (f). The normalization coefficient varies proportional to the Mach number for laminar and turbulent flow case. Once, the variation of the normalization coefficient is characterized, it is possible to compute the real shear stresses from the experimental data.

CONCLUSIONS

A new technique for quantitative measurements with oil flow visualization was evaluated. Reasonable results concerning wall shear stress calculations have been obtained.

The oil/pigment mixture chose for the oil dot visualization it's suitable for high flow speed cases (Mach>0.3). It shows a pseudoplastic behavior in certain velocity gradient ranges.

The validation tests on a flat plate in a free jet facility at different flow speeds allowed the development of the technique. Data analysis has been carried out by means of a suitable post processing tool. It allows the computation of the dot's surface, velocity and related wall shear stress based on the images analysis of oil dot deformations. The oil dot velocity is related to the velocity of the external flow. The wall shear stress measurements are in good agreement with the theoretical results by means of a normalization coefficient. It follows an increasing trend with the flow velocity.

This new technique is quite promising for the measurements of the wall shear stress and the flow speed.

ACKNOWLEDGMENTS

REFERENCES

[1] J. W. Naughton and M. Sheplak, August-October 2002, "Modern developments in shear stress measurement" Progress in Aerospace Sciences, Vol. 38, Pages 515-570.

[2] Q. Tian, R. L. Simpson and G. Tang, 2004, "Flow visualization on the linear compressor cascade endwall using oil flows and laser doppler anemometry" Measurement science and technology, Vol. 15, Pages 1910-1916.

[3] N. Atsushi, F. Nobuyuki, K. Eiichi and A. Tsuneo, 1999, "Visualization and image analysis of shear stress distribution over a fan blade" Journal of the visualization society of Japan, Vol. 19, Pages 137-140.

[4] J.W. Naughton, 2005, "High-Quality Skin Friction Measurements in 2-D Flows Using Oil Film Interferometry" Instrumentation in Aerospace Simulation Facilities, 21st International Congress, Pages 166–175.

[5] M. Ito and M. Oyangi, 1993, "Approximate estimation of skin friction by oil dot method" Journal of the visualization society of Japan, Vol. 13, Pages 179-182.

[6] L.C. Squire, 1961, "The motion of thin oil sheet under the steady boundary layer on a body" Journal of Fluid Mechanics, Vol. 11, Pages 161-179.

[7] L. H. Tanner and L. G. Blows, 1975, "A study of the motion of oil films on surfaces in air flow, with application to the measurement of skin friction" Journal of Physics E: Scientific Instruments, Vol. 9, Pages 194-202.

[8] J. L. Brown and J. W. Naughton, 1999, "The thin oil film equation" NASA/TM-1999-208767.

[9] H. Schlichting, 1968, "Boundary-Layer Theory".